Fibers and Polymers 2018, Vol.19, No.4, 914-926
DOI 10.1007/s12221-018-7839-2

ISSN 1229-9197 (print version)
ISSN 1875-0052 (electronic version)

Enhanced Flame Retardancy, Thermal and Mechanical Properties of Hybrid Magnesium Hydroxide/Montmorillonite Reinforced Polyamide 6/Polypropylene Nanocomposites

Reza Arjmandi[1], Harintharavimal Balakrishnan[1,2], Azman Hassan[1]*, Mohammad Jawaid[3], and Alothman Y. Othman[4]

[1]*Department of Bioprocess and Polymer Engineering, Faculty of Chemical and Energy Engineering, Universiti Teknologi Malaysia, Skudai 81310, Malaysia*
[2]*Trans Pacific Textile (M) Sdn Bhd (Prolexus Bhd), Jalan Mersing, Kluang 86000, Malaysia*
[3]*Department of Biocomposite Technology, Institute of Tropical Forestry and Forest Products (INTROP), Universiti Putra Malaysia, Serdang 43400, Malaysia*
[4]*Faculty of Chemical Engineering, King Saud University, Riyadh 11421, Saudi Arabia*
(Received September 26, 2017; Revised December 12, 2017; Accepted December 13, 2017)

Abstract: In this study, the effects of hybrid magnesium hydroxide/montmorillonite (MH/MMT) on the flame retardancy, thermal, mechanical, morphological and thermo-mechanical properties of polyamide 6/polypropylene (PA6/PP) nanocomposites prepared by melt blending technique were investigated. The partial replacement of MH with MMT (2 and 4 wt%) was done at total filler content of 30 wt% and maleated polypropylene was used as compatibilizer. Mass loss calorimeter analysis revealed that the peak heat release rate and total heat evolved values reduced in the presence of MMT due to the formation of the protective surface and insulation layer by MMT within the MgO layer formed on the surface upon combustion. The char residue also strengthened by migration of MMT layers to the surface of char. The thermal stability and flame retardancy of PA6/PP/MH/MMT nanocomposites improved with increasing MMT content. The MMT layers were well dispersed in the nanocomposites. The stiffness and toughness of PA6/PP/MH nanocomposites increased while the strength maintained with incorporation of MMT. The degree of crystallinity of both PA6 and PP increased with the addition of MMT while the melting point remained unaltered. The synergistic combination of MH and MMT has indeed maintained the mechanical properties of nanocomposites while further improving the flame retardancy.

Keywords: Polyamide 6/polypropylene, Magnesium hydroxide, Montmorillonite, Flame retardancy, Nanocomposites

Introduction

Recent advances in polymer composites technology have encouraged the replacement of metals in various applications especially in transportation, construction and oil and gas field. Polyamide (PA6) is the widely used engineering thermoplastic in a variety of high performance applications due to its inherent stiffness and strength over a broad temperature range with good wear, abrasion and chemical resistance [1]. However, for impact resistant applications, PA6 has proved to be notch sensitive and brittle at low temperatures, indicating poor resistance to crack propagation. Besides that, the hydrophilic nature of PA6 attributed to the presence of amide linkages in its structure makes PA6 vulnerable to moisture attack, which substantially led to hydrolytic degradation [2]. The introduction of polypropylene (PP) into PA6 has been investigated by previous researchers [3,4]. PP was used to tackle PA6's notch sensitiveness and the blending of a hydrophobic polymer as PP improved the moisture resistance properties of PA6 apart from resulting in reduction of overall production cost. Previous investigations showed that the use of maleated polypropylene (PPMA) as compatibilizing agent is vital to improve the compatibility between PA6 and PP [5,6].

Although PA6/PP blends may be well-established with improvements in terms of toughness and moisture resistance, there is still an urge to enhance its flame retardant properties to widen its applications in electronics, automotive and aerospace industries. Flame retardant agents are therefore can be used to attain higher ignition resistance with minimized flame spread, smoke suppression and containment of flame/ degradation products [7,8]. Halogen-free flame retardants such as magnesium hydroxide (MH) have been utilized as flame retardants for PA6 [9]. The formation of magnesium oxide act as a heat insulative layer to inhibit the migration of flammable volatile organic compounds into the vapor phase, and the formation of water as by-product also contributes positively to the dilution of the flammable vapor phase thus, reducing the heat of fire. Although the use MH as a substitute for halogen based flame retardants is seem to be feasible, MH is less effective and required high addition level (>20 wt%) in order to achieve acceptable flammability resistance [10]. Significant disadvantages of these filling levels are the lack of flexibility of the end products, poor mechanical properties and inconvenient compounding and processing steps. Synergistic combinations usually allow reductions of flame retardant loading, example include combinations of MH with layered silicates [11-14]. Song *et*

*Corresponding author: azmanh@cheme.utm.my

al. [13] reported that simultaneously use of montmorillonite (MMT) and MH improved the flame retardant properties of PA6 nanocomposites. Isitman *et al.* [14] also reported that the substitution of a certain fraction of the flame retardant with MMT significantly reduced the peak heat release rate values and delayed ignition time of PA6/MMT nanocomposites in cone calorimeter analysis. In addition, Lenza *et al.* [15] reported that the addition of hybrid MA/MMT into polyethylene nanocomposites increased the limiting oxygen index (LOI) at lower total flame retardants content while fulfilling the fire retardancy requirements. The addition of MMT also shorten times of ignition and reduce peak heat release rates to the formation of a surface layer which acts as mass and heat barrier to protect the underlying material from further burning. Recently, Kong *et al.* [16] reported that incorporation of only small amount of Fe-MMT into PP/MH composite resulted in better thermal stability and flame retardancy of nanocomposites, which indicated that MMT had a synergistic effect with MH. Therefore, it is a novel step to utilize MMT to replace MH content without sacrificing the flame retardant properties while maintaining inherent mechanical strength and toughness.

In our previous publication [17], MH flame retarded PA6/PP composite was developed with enhanced fire resistance performance at the expense of thermal stability, toughness, tensile and flexural strength. This subsequent part of the study focused on the simultaneously use of MH and MMT to improve the mechanical and thermal properties of PA6/PP nanocomposites. The partial replacement of MH with MMT is expected to avoid the deterioration of thermal and mechanical properties especially the strength and toughness of PA6/PP/MH nanocomposites while further enhancing or maintaining its inherent flame retardant properties. To the best of our knowledge, no study has been reported to investigate the flame retardancy, thermal and mechanical properties of PA6/PP nanocomposites in the presence of hybrid MH/MMT fillers. This study provides a new class of applications for nanofillers as weight replacement for halogen-free flame-retardant materials in PA6/PP nanocomposites.

Experimental

Materials

The PA6 was obtained from Toray Plastics Japan (product name Amilan CM1017-K) with melt mass flow rate (MFR) of 35 g/10 min at 230 °C and 2.16 kg load and density of 1.14 g/cm^3. The PP was obtained from Titan Chemicals, Malaysia (product name SM-240) with MFR at 230 °C and 2.16 kg load of 25 g/10 min and density of 0.96 g/cm^3. Silane-treated magnesium hydroxide (MH) with product name of Zerogen® 50SP was supplied by Huber Corporations. The PPMA, Orevac CA 100 with ~1 wt% of maleic anhydride (MA) which was used to promote adhesion between PA6 and PP was a product from ATOFINA, France. Organically modified MMT obtained from Nanocor Inc. Arlington Heights IL, USA (Nanomer 1.30TC) organically modified with octadecylamine with mean dry particle size of 16-22 μm.

Table 1. Compounding formulations for MH replacement with MMT in PA6/PP/MH nanocomposites

Designation	PA6/PP with the ratio of 70:30 (wt%)	PPMA (wt%)	MH (wt%)	MMT (wt%)
30 % MH	65	5	30	-
2MMT	65	5	28	2
4MMT	65	5	26	4

Nanocomposites Preparation

PA6 and PP pellets were dried at 60 °C for 24 hours prior to compounding. PA6/PP/MH nanocomposites and nanocomposites as listed in Table 1 was compounded by simultaneous addition of all components to Brabender Plasticoder P 2000 counter-rotating twin screw extruder. The barrel temperature profile adopted during compounding for all formulations was 190 °C at feed section, increasing to 240 °C at the die head. The screw rotation speed was fixed at 60 rpm. The extruded materials were injection molded into standard tensile, flexural and Izod impact specimens by using a JSW (Muraron, Japan) Model NIOOB II injection-molding machine with a barrel temperature range of 200-240 °C. All test specimens were left under ambient conditions in desiccators for at least 24 hours prior to testing. For mass loss calorimeter analysis, square samples with dimensions 100×100×3 mm^3 were prepared via compression molding.

Characterization of Nanocomposites

Flame Retardancy Analysis

The heat release rate (HRR) and mass loss rate (MLR) were determined using a mass loss calorimeter (Fire Testing Technology, UK) with conical radiant heater and thermopile detector conforming to ISO 13927 standards. Tests were performed under 50 kW/m^2 external radiant heat flux which corresponds to a mild-to-intermediate fire scenario. Thermopile temperature and sample mass data were recorded throughout combustion using a data acquisition system. Temperature readings were then converted to HRR using appropriate calibration curves obtained by burning a calibration gas fed into the sample compartment at various flow rates. Each studied formulation was tested twice and measured HRR and MLR were reproducible within ±10 %. Digital photographs of whole surfaces of burnt samples were also taken. LOI was determined according to ASTM 2863 on an FTT Oxygen index apparatus. Samples were also classified for their flammability resistance according to UL-94 standards at 3 mm thickness.

Mechanical Analysis

Tensile and flexural testing were conducted using an Instron (Bucks, UK) 5567 under ambient conditions according to ASTM D638 and ASTM D790, respectively. The crosshead speeds of 50 mm/min and 5 mm/min were used to tensile and flexural tests, respectively. Izod impact tests was done on notched impact samples (ASTM 256), using a Toyoseiki (Tokyo, Japan) impact testing machine under ambient conditions. Five specimens are tested and the average values being reported.

Thermal Analysis

The melting and crystallization behaviour of PA6, PA6/PP and PA6/PP/MH nanocomposites were characterized through differential scanning calorimetry (DSC) (Perkin-Elmer DSC-6), using 5-10 mg samples sealed in aluminium pans. The temperature was raised from 30 to 250 °C at a heating rate of 10 °C/min, and after a period of 1 min, it was swept back at 10 °C/min. The fusion enthalpies, ΔH_m ($PA6$) and ΔH_m (PP) were measured and the degree of crystallinity, X_c ($PA6$) and X_c (PP) were calculated using equation (1) and (2), respectively.

$$X_c(PA6) = \frac{\Delta H_m\,(PA6)}{\Delta H_m^0\,(PA6)} \times \frac{1}{w_{PA6}} \times 100\% \quad (1)$$

$$X_c\,(PP) = \frac{\Delta H_m\,(PP)}{\Delta H_m^0\,(PP)} \times \frac{1}{w_{PP}} \times 100\% \quad (2)$$

where, $\Delta H_m^0\,(PA6)$ =190.8 J/g and $\Delta H_m^0\,(PP)$ =209.2 J/g are the fusion enthalpies of 100 % crystalline PA6 and PP, respectively, and w_{PA6} and w_{PP} are the weight fractions of PA6 and PP, respectively [18]. PPMA was included in PP weight fraction.

In order to examine the thermal degradation behaviour of samples, thermogravimetric analysis (TGA) was performed on Perkin Elmer TGA 7 instrument at a rate of 10 °C/min under nitrogen atmosphere.

X-ray Diffraction Analysis

Siemens (Berlin, Germany) D5000 X-ray diffractometer was used to carry out X-ray diffraction (XRD) analysis. Patterns were recorded with a step size of 0.02 ° (2θ=2.0-10.0°). The interlayer distances (d-spacing) of the MMT in the nanocomposites was derived from the peak positions (d001 reflections) in the XRD graphs, according to the Bragg equation (3).

$$n\lambda = 2d\sin\theta_p \quad (3)$$

where, θ_p is diffraction angle of the primary diffraction peak and λ is X-ray wavelength. λ=0.154 nm (Cu Kα) and n=1 was used.

Morphological Analysis

JEOL JSM-6390 LV type scanning electron microscope (SEM) was used to observe the morphology of PA6, PA6/PP and PA6/PP/MH nanocomposites. All the SEM samples were Izod impact fractured perpendicular to the injection-molding direction at ambient conditions. Samples were coated with thin layer of platinum prior to examination under the electron beam. An operating voltage of 25 kV was used. For transmission electron microscopy (TEM) analysis, the samples were cut into trapezium shape of 1 mm^2 blocks. The sample was then fixed onto a Leica EM FC6 ultra-microtome for sectioning. Sections were cut at thickness of around 70-80 nm. The trimmed samples were taken out from the frozen chamber and deposited onto a copper grid wetted with propanol. The grid was then viewed under a TEM model LEOLIBRA 120 (Carl Zeiss) at 120 kV. The images were then taken.

Thermo-mechanical Analysis

The storage modulus (E'), loss modulus (E'') and tan delta (E''/E') curves as a function of temperature (T), was determined by dynamic mechanical thermal analysis by using a Perkin-Elmer DMA 7e instrument. DMA spectra were taken in the three-point bending mode, at a frequency of 1 Hz, over a broad temperature range (T=-110 to 100 °C) at a programmed heating rate of 5 °C/min. Samples with dimensions of 15×9×3 mm^3 was used for the test.

Results and Discussion

X-ray Diffraction

The X-ray diffraction (XRD) patterns of MMT, 2MMT and 4MMT are shown in Figure 1. The disappearance of the distinct d001 peak at 2θ=3.52 ° (2.5 nm) shows that the MMT layers are well dispersed in both 2MMT and 4MMT. This indicates that the presence of MH has little influence on the dispersability of MMT in PA6/PP matrix. The use of XRD to probe the distribution of MMT in PA6/PP has been reported in numerous previous studies [19-21]. The researchers reported that the disappearance of the distinct d001 peak shows enhanced distribution of MMT in PA6/PP.

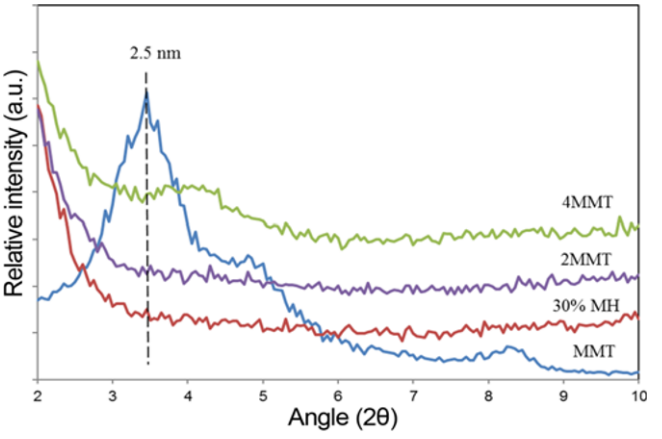

Figure 1. XRD curves of MMT, 30 % MH, 2MMT and 4MMT.

Morphological Properties

The SEM micrographs of impact fractured surface of 30 % MH, 2MMT and 4MMT are shown in Figures 2(a-f). The PP particles (as shown by arrows) can be seen to be well and uniformly dispersed throughout a rough fractured surface similar to the SEM micrographs of PA6/PP and PA6/PP/MH nanocomposites observed in earlier study [17]. Figure 2 also shows that the presence of MMT has decreased the particle size of PP in PA6/PP/MH composite. The magnified images also show that the particle size of PP further decreased with increasing MMT content. This is due to the coalescence suppression factor posed by MMT. Previous study by Balakrishnan *et al.* [22] also observed similar reduction in the particle size of polyethylene in PLA matrix with increasing addition of MMT. The magnified images also show that the smooth and well compatibilized interface of PP particles in PA6/PP as observed previously is not visible [17]. This indicates that the presence of MMT in PA6/PP/MH nanocomposites has minimal effect in improving the interfacial phase of PA6 and PP.

Figures 3(a)-(d) shows the TEM micrographs of 2MMT and 4MMT. The magnified TEM micrographs shown in Figures 3(b) and (d) confirm the presence of well dispersed individual MMT layers (as shown by arrows) which provides further support for the observations through XRD analysis earlier. Previous studies by Song *et al.* [13] and Dong *et al.* [23] also reported similar observation on the dispersion of MMT layers in PA6 matrix. On the other hand, studies by Varley *et al.* [24] and Samyn *et al.* [25] stressed that the role of MMT dispersion is vital for the improvement of flame retardancy behaviour of PA6/MMT nanocomposites. The researchers stated that excellent fire-retardant properties exhibited when good dispersion of MMT is achieved. It is worth to note that some MMT layers tend to locate itself around MH particles (Figure 3(d)) in 4MMT although the MMT layers were also seen to be well dispersed in PA6.

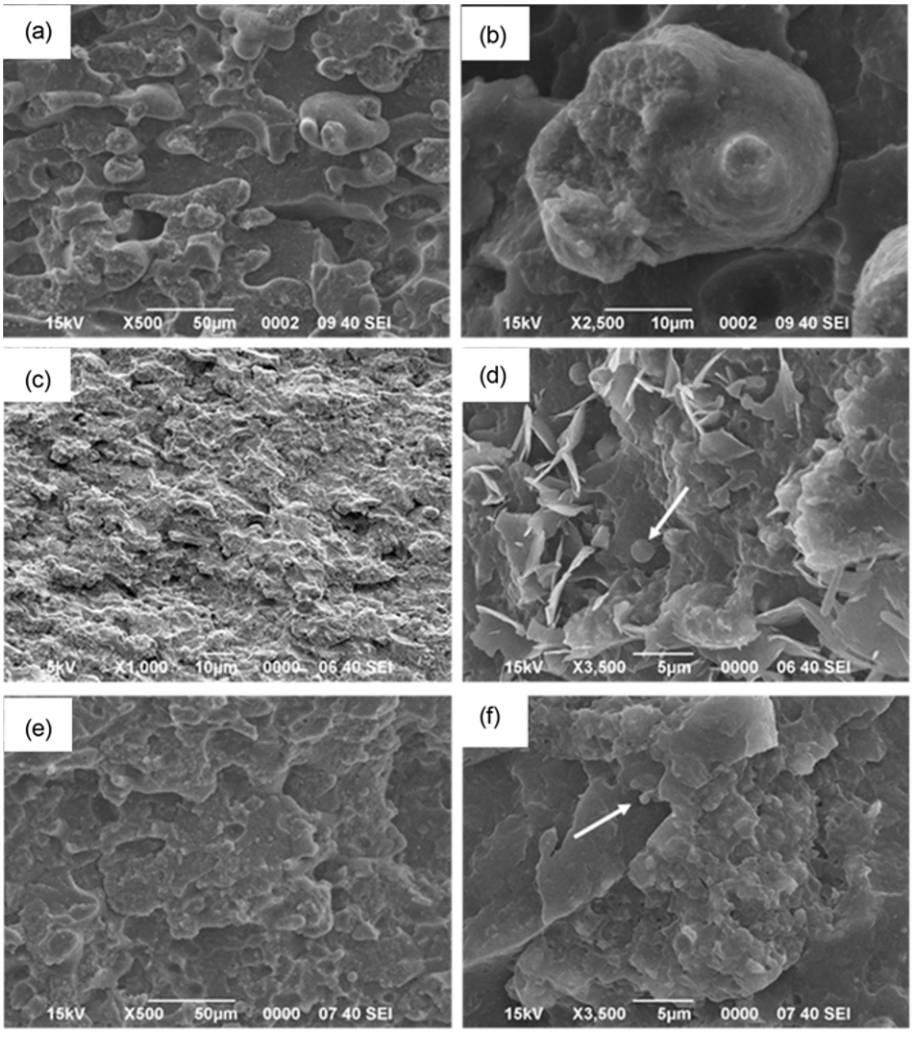

Figure 2. SEM micrographs of fractured surface of PA6/PP/MH nanocomposites and nanocomposites along with respective magnified images; (a, b) 30 % MH, (c, d) 2MMT, and (e, f) 4MMT.

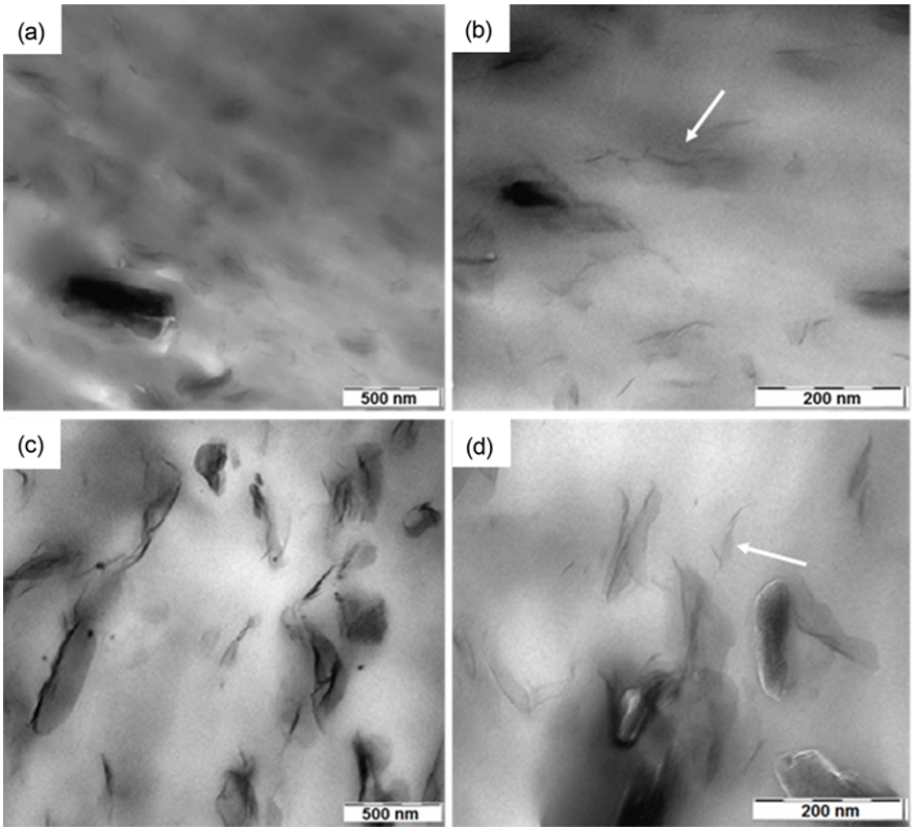

Figure 3. TEM micrographs of PA6/PP/MH nanocomposites along with respective magnified images; (a, b) 2MMT and (c, d) 4MMT.

Previous studies by Samyn *et al.* [26] who characterized the dispersion of MMT in polymer-flame retarded nanocomposites also reported the presence of MMT layers around OP1311 (a phosphorus based flame retardant) in PA6. Nevertheless, the well distributed MMT layers in the present study suggests that the presence of MH has little influence on the dispersion of MMT in PA6 matrix as confirmed by XRD analysis earlier.

Thermal Properties

Thermogravimetric (TG) and derivative thermogravimetric (DTG) curves of MMT, 30 % MH, 2MMT and 4MMT are shown in Figures 4(a) and (b), respectively. The initial thermal stability is characterized by the temperature at 15 % weight loss occurred referred to as $T_{15\%}$, is tabulated in Table 2. The TG and DTG curves of MMT in Figures 4(a) and (b) clearly indicates a higher thermal stability of MMT compared to PA6/PP/MH composite and nanocomposites. The total weight loss (around 30 %) in neat MMT which can be observed from Figure 4(b), is due to the decomposition of octadecylamine molecules. This is in agreement with previous study by Chow *et al.* [19] in PA6/PP/MMT nanocomposites. It can be seen from Figure 4(a) and Table 2 that the $T_{15\%}$ of 30 % MH filled PA6/PP composites increased significantly with the presence of MMT and the values increased further

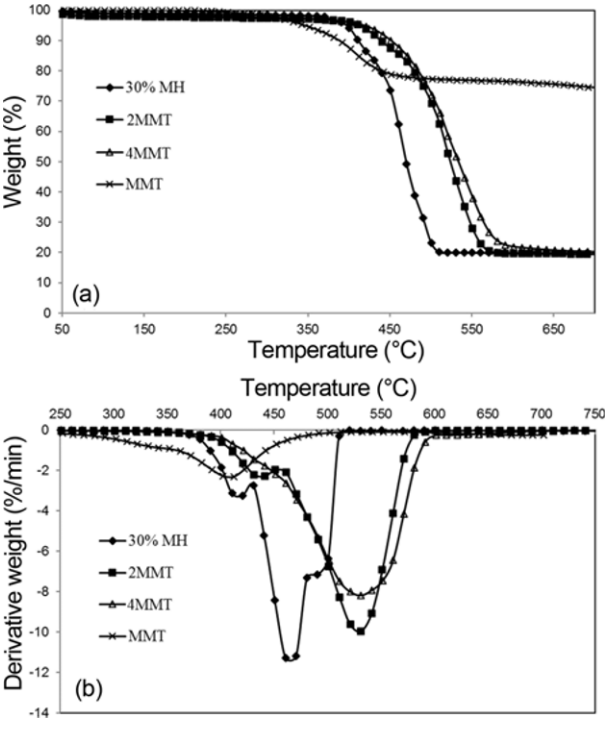

Figure 4. (a) TGA and (b) DTG curves of MMT, 30 % MH, 2MMT and 4MMT.

Table 2. TGA characterization and residue values

Designation	$T_{15\%}$ (°C)	Residue at 650 °C (%)
30 % MH	422.1	19.80
2MMT	461.1	19.71
4MMT	470.2	20.75

with increasing MMT content. It is deduced that the improved thermal stability for PA6/PP/MH nanocomposites is attributed to the presence of MMT which hinders the out-diffusion of the volatile decomposition products directly leading to decreased permeability. The higher thermal stability of MMT may have also contributed to the higher $T_{15\%}$ of PA6/PP/MH nanocomposites. Previous study by Othman *et al.* [3] also reported similar observations.

The early decomposition of 30 wt% MH filled PA6/PP composite as shown in Figure 4(b) is due to endothermic decomposition of MH to magnesia (MgO) and water at ~380 °C as discussed previously by Balakrishnan *et al.* [17] As observed from the DTG curves in Figure 4(b) the decomposition of MH starts at 360 °C reaching its maximal weight loss at ~430 °C while PA6 recorded maximal decomposition at 480 °C [9]. The replacement of MH with MMT in PA6/PP/MH nanocomposites has shifted the maximal decomposition temperatures of both MH and PA6 to higher temperatures. The presence of MMT also reduced the derivative weight loss peak of MH and PA6 which shows a lower rate of evolution of volatile decomposition products during degradation. Figure 4(b) also shows that the increasing MMT content has resulted in higher maximal decomposition temperatures and lower the derivative weight loss peak. It can be said that apart from the presence of MgO layer upon decomposition of MH, the MMT layers also made a positive contribution in the retardation of the escape of volatile decomposition products into the gas phase. It is believed that the MMT layers may also impede the volatile evolution via a torturous pathway due to the large aspect ratio of MMT layers. Thus, it can be stated that the drastic reduction in the peak of derivative weight loss in PA6/PP/MH nanocomposites is due to the combined effect of both MH and MMT which indicates further improvement in flame retardancy. Previous study by Isitman *et al.* [14] also revealed a lower peak of derivative weight loss peak of PA6 with the use of MMT in flame retarded/glass fibre reinforced PA6 nanocomposites. The researchers documented that the ability of MMT to impede the release of volatile decomposition products which combustible could play a vital role in flame retardancy of polymer composites and nanocomposites. Other studies also documented further reduce in the peak of derivative weight loss of PA6 in PA6/MMT nanocomposites with increasing MMT content [24,27,28].

The residue weight at 650 °C for MMT, 30 % MH, 2MMT and 4MMT are also tabulated in Table 2. The remaining residue of MH filled PA6/PP formulations is mainly attributed to the formed MgO as the dehydration product of MH which resulted in weight loss of ~30 % as discussed earlier. It is interesting to note that the total residue weight percentage of PA6/PP/MH nanocomposites did not undergo significant change despite the reduction in weight fraction of MH. This is due to the residue weight by MMT itself which compensated the weight fraction of MgO originating from MH. The residue weight data indicates that the presence of MMT layers in residue upon decomposition of polymer matrices has led to the formation of inorganic chars. The ability of MMT to form residue upon degradation is well documented by previous studies by Varley *et al.* [24], Kashiwagi *et al.* [27] and Leszczyńska *et al.* [29].

Flammability and Fire Properties

The heat release rate (HRR) and total heat evolved (THE) curves of 30 % MH, 2MMT and 4MMT are shown in Figures 5(a) and (b), respectively. It can be observed that the MH replacement with MMT further decreased both HRR and THE values of 30 % MH. The HRR and THE curves also indicates that the PA6/PP/MH nanocomposites has undergone slow and nearly complete burning along with further decrease in HRR and THE values observed at higher

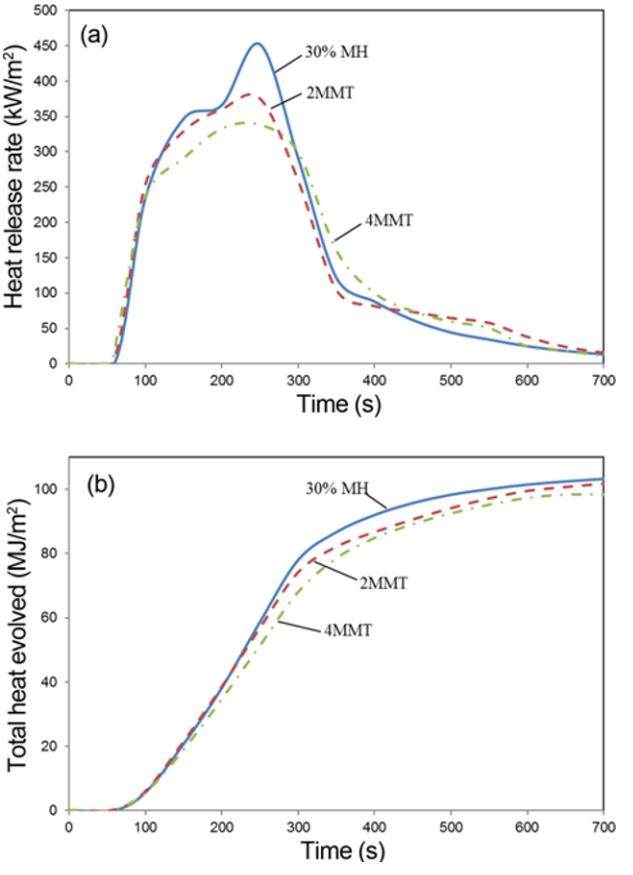

Figure 5. (a) HRR and (b) THE curves of 30 % MH, 2MMT and 4MMT.

MMT content. The reduction in HRR and THE values is due to the formation of the protective surface and insulation layer by MMT within the MgO layer formed on the surface upon combustion. The significant reduction in HRR and THE values of 4MMT suggest that the insulation effect is enhanced further with increasing MMT content. Thus, it can be said that the synergistic combination of MH and MMT has resulted in an improved flame retardancy in PA6/PP nanocomposites. Previous investigations by Haurie *et al.* [30] and Laoutid *et al.* [31] on similar synergistic effect of MH and MMT reported that the presence of MMT in association with hydrated minerals significantly decreased the HRR value in cone calorimeter test.

The synergistic flame retardant effect of MH and MMT in ethylene-vinyl acetate copolymer (EVA) was investigated by Yen *et al.* [32]. The researchers found that MMT filled EVA/MH nanocomposites exhibited better flame retardancy properties in comparison to EVA/MH composites. Another study by Marosfoi *et al.* [33] also reported on the synergistic flame retardancy effect of MMT and MH in PP. It was concluded that the post-combustion interaction between MH and MMT played a key role in fire retardant mechanism. Previous studies by Samyn *et al.* [25], Zhang *et al.* [34] and Bourbigot *et al.* [35] also reported that the decreasing HRR values with the addition of MMT in PA6 is a vital trait of improved flame retardancy. The ability of MMT to act as barriers and create a torturous pathway for the evolution of volatile combustible to the flaming zone also plays a role in the reduction of HRR of PA6/PP/MH nanocomposites. The barrier effect posed by MMT layers is well documented in a literature review by Leszczyńska *et al.* [29] and Gilman [36].

The peak mass loss rate (PMLR) values of 30 % MH, 2MMT and 4MMT are tabulated in Table 3. The PMLR value of 30 % MH decreased with MH replacement with MMT and the PMLR value deteriorated further with increasing MMT content. It appeared that the MMT layers also acted as mass transport barrier which subsequently leads to improved flame retardancy and suppressed pyrolysis. This is in agreement with previous observations by Isitman *et al.* [14] and Gilman [36]. Studies by Song *et al.* [13] and Yen *et al.* [32] also stressed that the combination of MgO and MMT form a stable char layer. The stable physical protective barrier on the surface during combustion insulates polymer matrix from heat source. The time to ignition (T_{ign}) values are also tabulated in Table 3. The earlier T_{ign} values and increasing HRR (Figure 5(a)) of PA6/PP nanocomposites at the early part of combustion are due to the combustion of octadecylamine group in MMT as discussed by previous studies [14,24,37]. Isitman *et al.* [14] reported that the MMT filled PA6/glass fibre nanocomposites ignited earlier than PA6/glass fibre composites as a result of acid catalysed degradation of PA6. Table 3 also shows the fire growth index (FGI) values of 30 % MH, 2MMT and 4MMT where, FGI is defined by the ratio of PHRR/T_{ign}. It can be observed that the MH replacement with 2 and 4 wt% of MMT in PA6/PP/MH nanocomposites has reduced the FGI value of 30 % MH. This shows that the presence of MMT has reduced the flame spread attributes of 30 % MH. Isitman *et al.* [14] also reported a decreased FGI value with similar approach by 5 wt% substitution of flame retardant with MMT in flame retarded PA6/glass fibre nanocomposites.

The mechanism of flame retardancy in MMT filled PA6/PP/MH nanocomposites can be analysed further by the ratio of THE/TML. This ratio allows for the deduction of availability of gas phase mechanism as it is a suitable measurement for the effective heat of combustion (ΔH_c) of volatiles [16]. It can be observed from Table 3 that the ΔH_c values of 30 % MH did not change significantly with the presence of MMT. The average value of 3.40 MJ/m^{2}g for 30 % MH becomes 3.36 MJ/m^{2}g on the average for 2MMT and 3.33 MJ/m^{2}g on the average for 4MMT. It should be noted that the change is well being in the range of experimental error margin. Thus, by considering the reduction in PHRR, PMRR and the unaltered ΔH_c values, it can be said that the condensed phase flame retardancy is enhanced in the presence of MMT, merely due to the formation of MMT reinforced MgO barrier (as investigated in the following section). Previous studies by Isitman *et al.* [14] and Schartel and Hull [38] agreed that the unchanged ΔH_c values is an indicator of condensed phase flame retardancy mechanism which is indeed predominant with the use of MMT. Another study by Varley *et al.* [24] also stated that the source of flame retardancy mechanism imposed by MMT remains within the condensed phase regardless of the distribution of MMT in polymer matrices, i.e. exfoliated or intercalated.

Figures 6(a)-(f) shows the SEM micrographs of fire residues of 30 % MH, 2MMT and 4MMT at two different magnifications to highlight the variation of char micro-

Table 3. Interpretation of mass loss calorimeter data

Designation	T_{ign} (s)	PHRR (kW/m^2)	PMLR (g/m^{2}s)	FGI (kw/m^2·s)	THE (MJ/m^2)	Δh_c (MJ/m^{2}g)
	± 5 %	± 6 %	± 8 %	± 1 %	± 4 %	± 5 %
30% MH	60	452	8.71	7.53	103.2	3.40
2MMT	58	384	7.24	6.62	101.7	3.36
4MMT	57	363	5.72	6.37	98.93	3.33

T_{ign}: time to ignition, PHRR: peak heat release rate, PMLR: peak mass loss rate, FGI: fire growth index, THE: total heat evolved and Δh_c: effective heat of combustion.

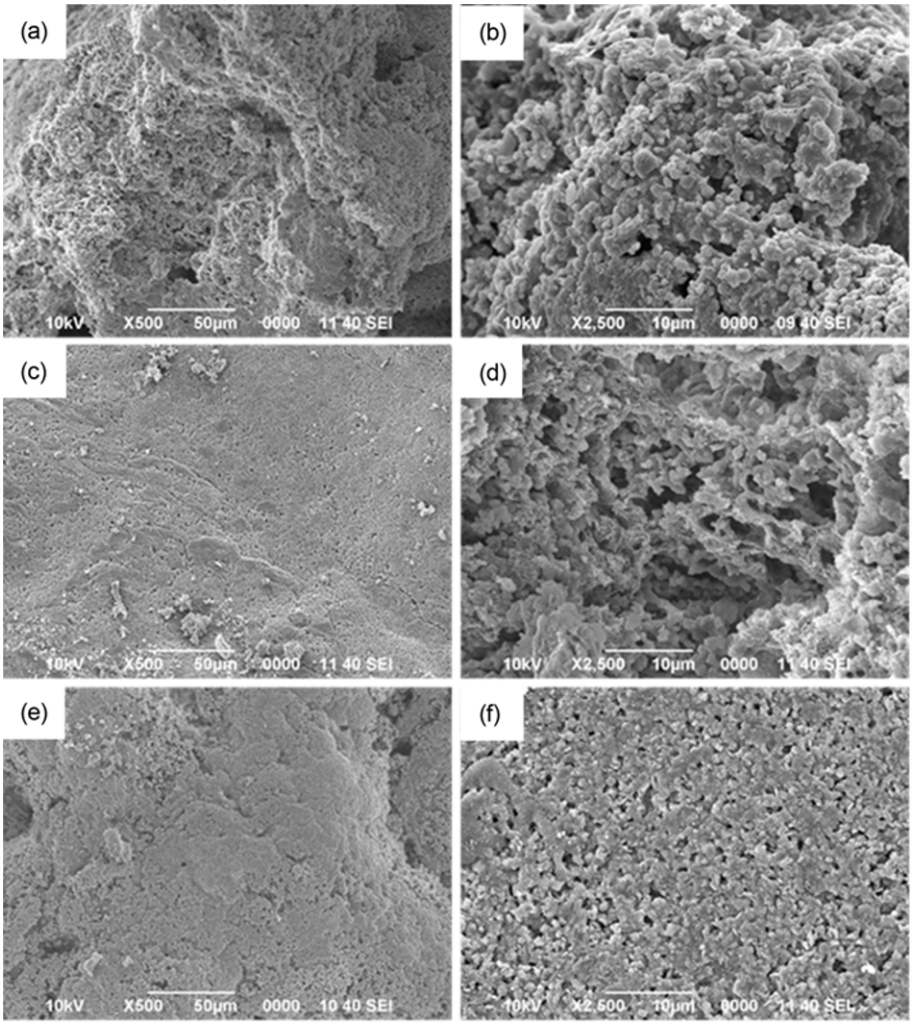

Figure 6. SEM micrographs of residue along with respective magnified images; (a, b) 30 % MH, (c, d) 2MMT, and (e, f) 4MMT.

structures on different length scales. The SEM micrographs (Figures 6(a) and (b)) of 30 % MH shows that the charred residue forms loose porous net structure after burning. It can be clearly observed that the charred residue of MMT filled PA6/PP/MH nanocomposites (Figures 6(c)-(f)) are more compact than that of 30 % MH. The number and size of holes also decreased along with increasing MMT content. Moreover, the study of the microstructure of the PA6/PP/MH nanocomposites residues show that the surface of the residue is more homogenous and compact. These findings imply that MMT promotes the formation of a homogenous and dense looking surface. Thus, it can be said that the homogenous compact char residue layer protects the underlying polymeric substrate from the heat source and slows down heat and mass transfer between the gaseous and condensed phases more effectively. This may have led to the reduced HRR, THE and PMLR values as discussed earlier.

It is believed that the char residue has also been strengthened by the migration of MMT layers to the surface of char. The migration of MMT to the surface of char residue, to act as insulator and reinforcing agent of char residue has been discussed in detail in previous studies [24,39,40]. XRD analysis is used to probe the distribution of MMT in char residue. The XRD curves of MMT and respective char residue of 30 % MH, 2MMT and 4MMT are shown in Figure 7. Interestingly, the absence of the distinct d001 peak at $2\theta=3.52^{o}$ (2.5 nm) in char residues of PA6/PP/MH nanocomposites shows that the MMT layers remain well dispersed in MgO char layer. Similar finding has been reported previously by Liu [12], Kong *et al.* [16] and Lu *et al.* [41] who found the disappearance of the d001 reflection peak derived from the interlayer spacing of MMT in nanocomposite samples, suggesting that the silicate layers had lost their reciprocal order, and almost complete exfoliation of clay had taken place. In addition, the presence of MgO has played a positive role in the distribution of MMT in char residue. The MgO has restricted the agglomeration of MMT in char residues upon combustion leading to the formation of

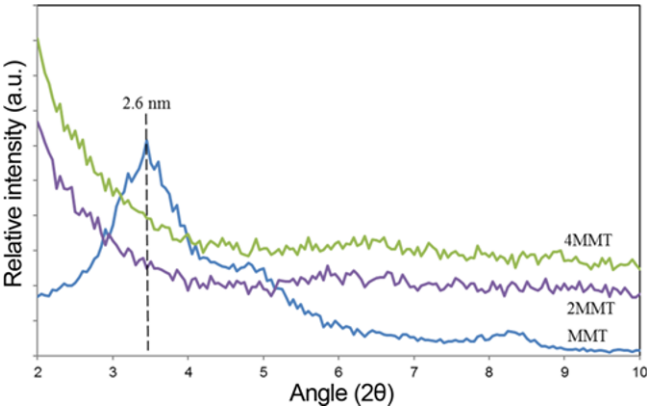

Figure 7. XRD curves of MMT and respective char residues of 2MMT and 4MMT.

more compact and uniform char microstructures as observed in Figures 6(c)-(f). This is in agreement with previous investigation by Isitman *et al.* [14] who also observed an exfoliated MMT distribution even after combustion, in the presence of a flame retardant which enhanced charring in glass fibre reinforced PA6 nanocomposites. It was stated that this could be due to the formation of a stable residue within the MMT galleries during flaming combustion. The stable residue has enabled the initially well dispersed MMT in PA6 to remain exfoliated within MgO char even after combustion.

Table 4 shows that the LOI value of 30 % MH improved gradually with MH replacement with 2 wt% of MMT. The LOI value was seen to further improve with increasing MMT content. It is believed that the enhanced LOI value is due to the presence of MMT in char which insulated the underlying polymer from heat while reducing the rate of diffusion of oxygen into the matrix. Previous studies by Isitman *et al.* [14] and Hao *et al.* [42] also reported similar increment in LOI value with the introduction of MMT. In addition, the UL-94 ratings of 30 % MH, 2MMT and 4MMT are also tabulated in Table 4. It can be observed that the MH replacement with 2 wt% of MMT maintained the UL-94 ratings of 30 % MH at V1 rating prior to a diminished V2 rating with increasing MMT content (4MMT). The dripping which ignited the cotton indicator in 4MMT also shows its poor performance in UL-94. The burned UL-94

Table 4. LOI values and UL-94 ratings of 30 % MH, 2MMT and 4MMT

Designation	LOI	UL-94	
		Rating	Drip
30 % MH	27.2	V-1	No
2MMT	29.8	V-1	No
4MMT	31.8	V-2	Yes[ig]

ig: ignited cotton indicator.

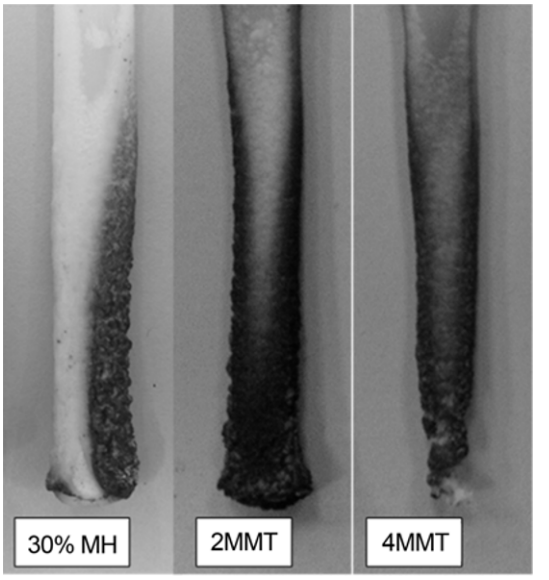

Figure 8. Appearance of UL-94 burned samples.

samples are shown in Figure 8. Nevertheless, the effect of MH replacement with MMT on the flame retardancy of 30 % MH were seen to contradict with the improvements observed through cone calorimetry and LOI analysis earlier due to the stringent ignition conditions and geometry of UL-94 as discussed previously by Isitman *et al.* [14] and Hu *et al.* [43].

Mechanical Properties

The effect of MH replacement with MMT on the mechanical properties of 30 % MH is shown in Figures 9(a)-(c). The MH replacement with MMT (2 and 4 wt%) has improved the overall mechanical strength of 30 % MH. Figures 9(a) and (b) show that both Young's and flexural modulus improved while the tensile and flexural strength maintained with increasing additions of MMT. It is well known that MMT pose reinforcing effect to the polymer matrix due to its higher stiffness along with high specific surface area as mentioned by Pavlidou and Papaspyrides [44]. The well dispersed MMT layers as observed from XRD and TEM analysis (Figures 1 and 3, respectively) earlier have played a vital role in the improvement of modulus and strength of PA6/PP/MH nanocomposite. When MMT layers are dispersed in intercalated and/or exfoliated form, it could lead to a higher aspect ratio of MMT layer, subsequently a larger exposed interfacial area between MMT and PA6. Both of these aforementioned factors could make the stress transfer to the MMT layers more effective subsequently improving the mechanical properties of the formed nanocomposites. Previous study by Chow *et al.* [45] also reported that the tensile strength of PA6/PP increased 18 % while Young's modulus improved by 13 % with the addition of 4 parts per hundred (phr) of MMT. Figure 9(c) shows that the impact strength and elongation at break of

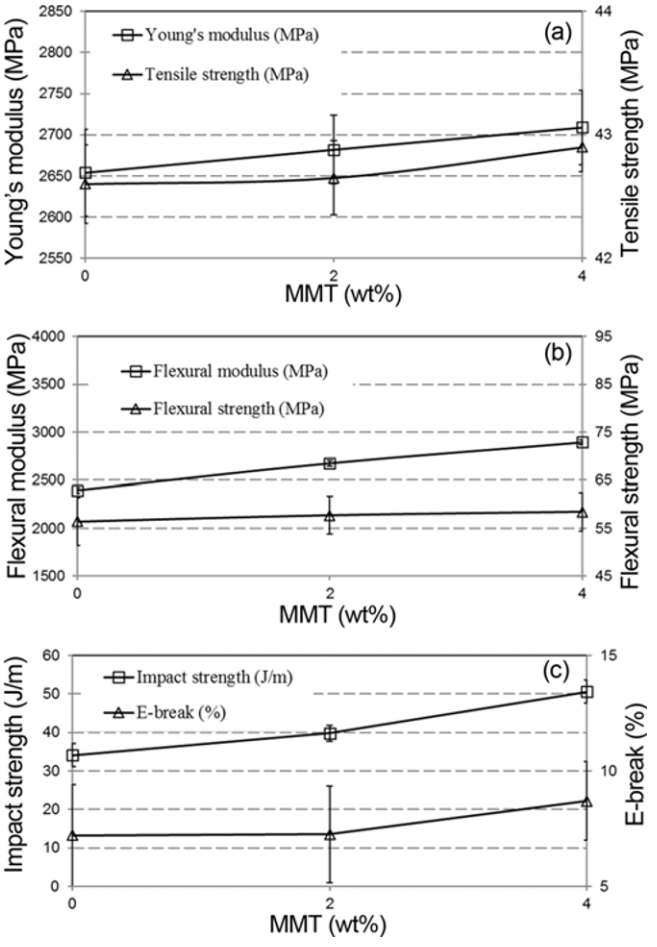

Figure 9. The effect of MH replacement with MMT on the mechanical properties of 30 % MH; (a) tensile strength and modulus, (b) flexural strength and modulus, and (c) impact strength and elongation at break.

30 wt% MH filled PA6/PP composite also improved slightly with the addition of MMT. The enhanced toughness in the present study is attributed to the good degree of dispersion of MMT as observed earlier (Figures 1 and 3) as the applied energy is well dissipated by the MMT layers. This is in agreement with previous studies by Kim *et al.* [46] and LePluart *et al.* [47].

Crystallization Behaviour

Table 5 tabulates the crystallization temperature (T_c), melting temperature (T_m), and degree of crystallinity (X_c) obtained from DSC analysis for 30 % MH, 2MMT and 4MMT. It can be observed that the X_c and T_c of both PA6 and PP increased with the presence of MMT. It is believed that MMT platelets acted as nucleating agents promoting the growth of crystals. The ability of MMT platelets to provide nucleation site for the growth of crystals is well documented in the literatures [48,49]. The increased nucleating sites induced the formation of polymer crystals indirectly influencing the crystallization to occur at higher temperatures during cooling. Previous studies by Lim *et al.* [50] and Balakrishnan *et al.* [51] also found that the T_c and X_c of PP increased with the addition of MMT. The T_m of both PA6 and PP however, remained unaltered. A study by Wahit *et al.* [21] who investigated the crystallization behaviour of polyoctene ethylene toughened PA6/PP/MMT nanocomposites also found that the addition of MMT has little effect on the T_m of PA6.

Thermo-mechanical Properties

Figures 10(a) and (b) show the storage modulus (E') and tan δ curves of 30 % MH, 2MMT and 4MMT over the temperature range of -110 to 100 °C, respectively. A gradual decline was observed in E' with increasing temperature from -110 to 100 °C (Figure 10(a)). The MH replacement with MMT improved the stiffness of 30 % MH throughout the temperature range due to restriction of chain mobility during deformation. This is supported by the increase in tensile and flexural modulus shown in Figures 9(a) and (b), respectively. Similar observation was reported by Chow *et al.* [19] in PA6/PP nanocomposites with the addition of MMT. The tan δ curve in Figure 10(b) illustrates two transition temperatures at ~30 °C and ~-70 °C for all the samples. The peak at ~30 °C is assigned to the α-relaxation peak due to the breakage of hydrogen bonds between the polymer chains which indirectly induces long range segmental motion in the amorphous region. Meanwhile, the broad peak at ~-70 °C corresponds to the β-relaxation peak of PA6 traced to segmental amide groups in the amorphous area which do not participate in hydrogen bonding. The observation is in agreement with a previous study by Tomova *et al.* [52]. A broader peak is observed for PA6/PP in the temperature range of 20-30 °C attributed to the overlapping of T_g of PP around 18 °C [51]. It should be noted that the addition of MMT did not significantly affect the tan δ values at lower temperature (~-70 °C).

Table 5. DSC data for 30 % MH, 2MMT and 4MMT

Designation	Crystallization temperature (T_c) (°C)		Melting temperature (T_m) (°C)		Crystallinity (X_c) (%)	
	PA6	PP	PA6	PP	PA6	PP
30 % MH	186	131	218	164	19.11	12.71
2MMT	187	130	218	164	24.20	15.94
4MMT	187	130	218	164	27.73	17.82

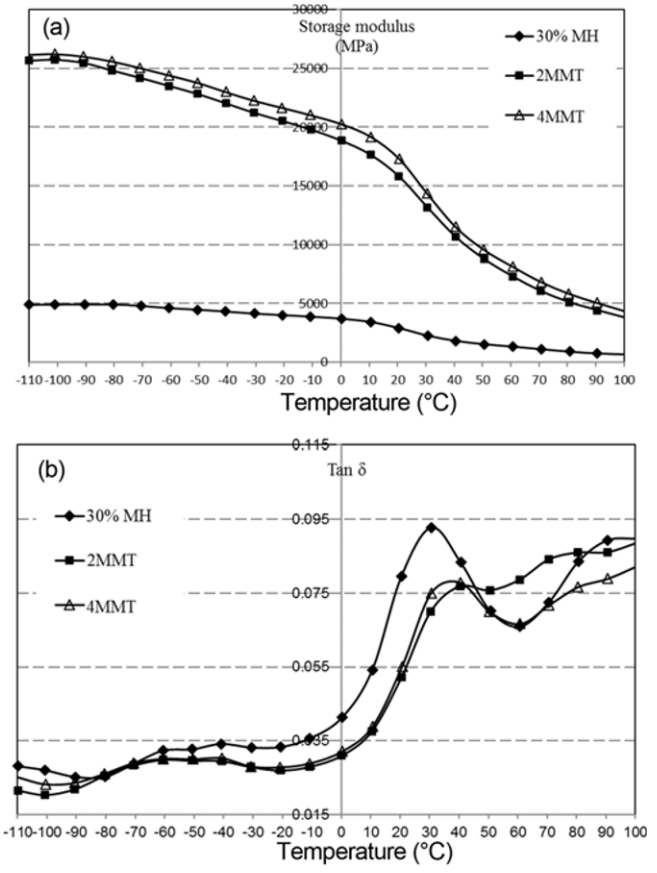

Figure 10. (a) Storage modulus and (b) Tan δ curves of 30 wt% MH filled PA6/PP composite and MMT filled PA6/PP/MH nanocomposites.

However, the lowering and shifting of tan δ peak (~25 °C) to higher temperature indicates that MMT restricts the mobility of PA6 chains which again can be related to the stiffening effect of MMT as discussed earlier. Chow *et al.* [19,45] also observed similar trend through the stiffening effect of MMT in PA6/PP/MMT nanocomposites.

Proposed Flame Retardancy Mechanism

Based on the observations in the present study, the aim of this section is to discuss the flame retardancy mechanism involved in PA6/PP/MH nanocomposites. Figure 11 shows a schematic diagram representing the morphology of nanocomposites, prior and subsequent to ignition. It can be observed that the ignition process has resulted in the formation of several layers during combustion ie; flame zone, residue layer, molten layer and solid layer. The molten layer represents the melting zone of polymer matrix due to intense heat from the flame zone. It is apparent that the decomposition of MH has resulted in the formation of MgO layer in the residue layer. The MgO layer acts as a barrier layer which hinders the out-diffusion of volatile combustible decomposition products to the flame zone. The MgO layer also insulates the molten layer from the heat of the flame.

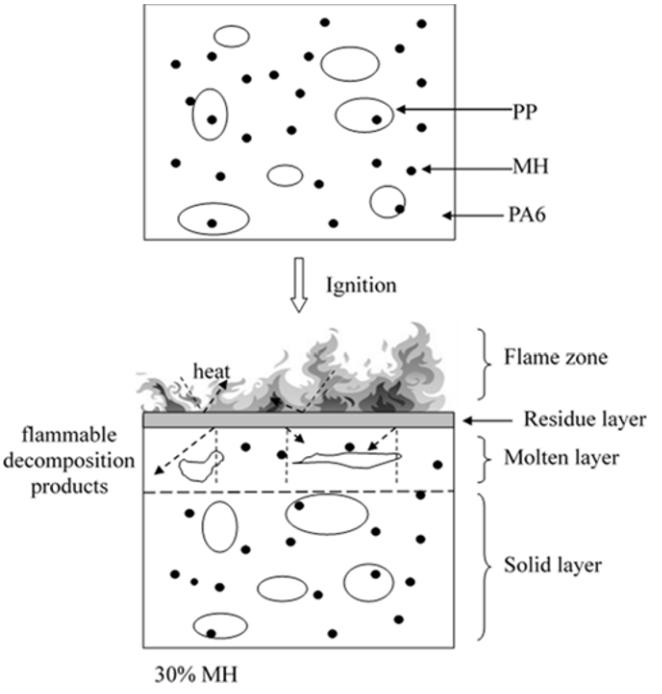

Figure 11. A schematic diagram representing the morphology of PA6/PP/MH nanocomposites, prior and subsequent to ignition.

Figure 12 illustrates a schematic diagram on the effect of MH replacement with 2 and 4 wt% of MMT in 30 % MH, prior and subsequent to ignition. It is clear that the mechanism of flame protection involves the formation of thicker and more compact residue layer acting as an insulating barrier while reducing the escape of volatile decomposition products to the flame. The formation of such residue layer during burning is critical in order to obtain a low heat release rate. It should be noted that the thickness of the residue layer also increased with increasing MMT content. The MMT platelets were also deduced to be well dispersed in the residue layer contributing to enhanced strength and thermal stability of the layer. In addition, the presence of MMT platelets also impedes the out-diffusion of decomposition products to the flame zone through the establishment of torturous pathways for out-diffusion.

The investigation on MH replacement with MMT showed a positive research approach to further improve the flame retardancy of 30 % MH while maintaining the mechanical strength of the nanocomposites. This is important to exhibit the relevance of the research approach despite the significant advantage displayed by 40 and 50 % MH over 30 % MH in terms of flame retardancy as observed earlier [17]. It is worth to mention that the deterioration of mechanical and impact strength may limit the potential application of MH flame retarded PA6/PP. The current research idea for MH replacement with MMT has indeed maintained the mechanical and impact strength of PA6/PP/MH nanocomposites while

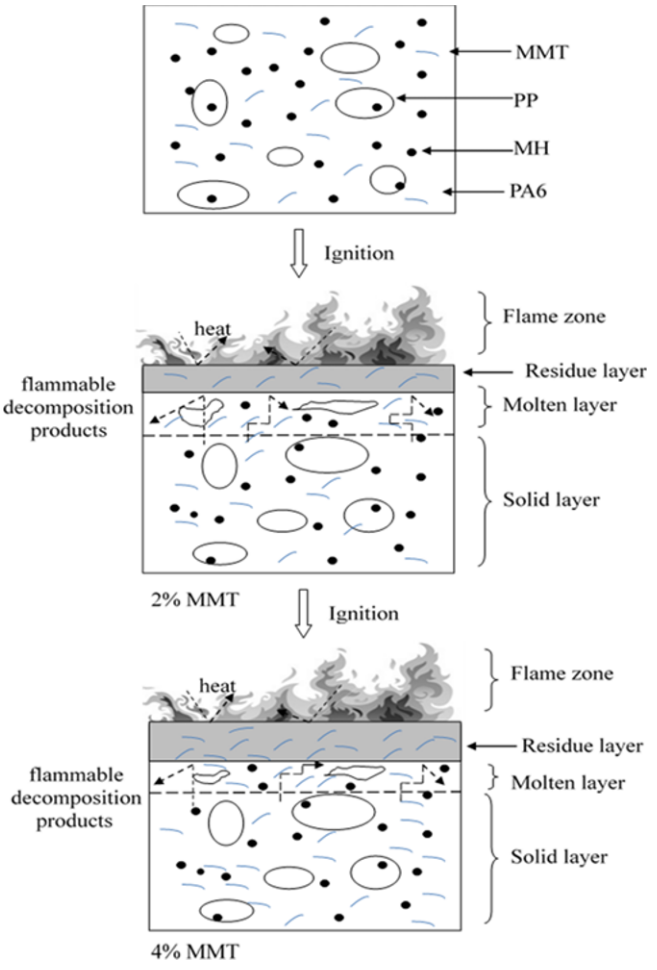

Figure 12. A schematic diagram on the effect of MH replacement with 2 wt% (2MMT) and 4 wt% MMT (4MMT) in 30% MH, prior and subsequent to ignition.

further improving the flame retardancy property. It is also evident that MMT has displayed a synergistic effect with MH to enhance the flame retardancy of MH flame retarded PA6/PP nanocomposites.

Conclusion

The effects of partial replacement of MH with MMT on the flame retardancy, thermal, mechanical, morphological and thermo-mechanical properties of PA6/PP/MH nanocomposites prepared by melt blending method were investigated. XRD analysis and TEM micrographs confirmed the presence of well dispersed individual MMT layers in PA6/PP/MH nanocomposites. TGA analysis showed that the thermal stability of PA6/PP/MH nanocomposites improved with increasing MMT content. The reduction in PHRR and THE values in the presence of MMT was achieved due to the formation of the protective surface and insulation layer by MMT within the MgO layer formed on the surface upon combustion. The synergistic combination of MH and MMT has resulted in an improved flame retardancy in PA6/PP nanocomposites. The LOI value increased with increasing MMT content while 4MMT registered poor UL-94 rating due to dripping behaviour. In addition, both Young's and flexural modulus of nanocomposites improved while the tensile and flexural strength maintained with increasing MMT content. The impact strength and elongation at break of PA6/PP/MH nanocomposite also improved slightly with the addition of MMT. Storage modulus revealed that the presence of MMT improved the stiffness of PA6/PP/MH nanocomposite throughout the temperature range (-110 to 100 °C) due to restriction of chain mobility during deformation. The exploration of MH replacement with MMT filler revealed the potential combined use of MH and MMT to improve the flame retardancy and thermal properties of PA6/PP while maintaining its mechanical strength.

Acknowledgement

The authors would like to thank Universiti Teknologi Malaysia (UTM) as well as Ministry of Higher Education for a Fundamental Research Grant Scheme (FRGS) Grant 78467. A line of appreciation to Ministry of Science, Technology and Innovation (MOSTI), Malaysia for the award of National Science Fellowship (NSF) scholarship for Harintharavimal Balakrishnan.

References

1. J. A. Brydson, "Plastics Materials", pp.487-493, Butterworth-Heinemann, 1999.
2. A. Dasari, Z. Z. Yu, Y. W. Mai, and S. Liu, *Nanotechnology*, **18**, 445 (2007).
3. N. Othman, A. Hassan, A. R. Rahmat, and M. U. Wahit, *Int. J. Polym. Mater.*, **56**, 893 (2007).
4. Z. A. Ishak, W. S. Chow, and T. Takeichi, *Polym. Compos.*, **31**, 1156 (2010).
5. E. Adem, G. Burillo, M. Avalos-Borja, and M. P. Carreón, *Nucl. Instr. Meth. Phys. Res. B*, **236**, 295 (2005).
6. M. U. Wahit, A. Hassan, Z. A. Mohd Ishak, and A. Abu Bakar, *Polym. Polym. Compos.*, **13**, 795 (2005).
7. M. Bar, R. Alagirusamy, and A. Das, *Fiber. Polym.*, **16**, 705 (2015).
8. S. Y. Lu and I. Hamerton, *Prog. Polym. Sci.*, **27**, 1661 (2002).
9. P. R. Hornsby, J. Wang, R. N. Rothon, G. Jackson, G. Wilkinson, and K. Cossick, *Polym. Degrad. Stabil.*, **51**, 235 (1996).
10. M. Ba, B. Liang, and C. Wang, *Fiber. Polym.*, **18**, 907 (2017).
11. A. Ahamad, C. B. Patil, P. P. Mahulikar, D. G. Hundiwale, and V. V. Gite, *J. Elastom. Plast.*, **44**, 251 (2012).
12. S. P. Liu, *J. Ind. Eng. Chem.*, **20**, 2401 (2014).

13. L. Song, Y. Hu, Z. Lin, S. Xuan, S. Wang, Z. Chen, and W. Fan, *Polym. Degrad. Stabil.*, **86**, 535 (2004).
14. N. A. Isitman, H. O. Gunduz, and C. Kaynak, *Polym. Degrad. Stabil.*, **94**, 2241 (2009).
15. J. Lenza, K. Merkel, and H. Rydarowski, *Polym. Degrad. Stabil.*, **97**, 2581 (2012).
16. Q. Kong, H. Wu, H. Zhang, X. Zhang, W. Zhao, and J. Zhang, *J. Nanosci. Nanotechnol.*, **16**, 8287 (2016).
17. H. Balakrishnan, A. Hassan, N. A. Isitman, and C. Kaynak, *Polym. Degrad. Stabil.*, **97**, 1447 (2012).
18. Z. M. Ishak, W. S. Chow, and T. Takeichi, *Eur. Polym. J.*, **44**, 1023 (2008).
19. W. S. Chow, Z. M. Ishak, J. Karger-Kocsis, A. A. Apostolov, and U. S. Ishiaku, *Polymer*, **44**, 7427 (2003).
20. M. U. Wahit, A. Hassan, A. R. Rahmat, and Z. M. Ishak, *J. Elastom. Plast.*, **38**, 231 (2006).
21. M. U. Wahit, A. Hassan, Z. M. Ishak, A. R. Rahmat, and A. A. Bakar, *J. Thermoplast. Compos. Mater.*, **19**, 545 (2006).
22. H. Balakrishnan, A. Hassan, M. U. Wahit, A. A. Yussuf, and S. B. A. Razak, *Mater. Des.*, **31**, 3289 (2010).
23. W. Dong, X. Zhang, Y. Liu, Q. Wang, H. Gui, J. Gao, Z. Song, J. Lai, F. Huang, and J. Qiao, *Polymer*, **47**, 6874 (2006).
24. R. J. Varley, A. M. Groth, and K. H. Leong, *Compos. Sci. Technol.*, **68**, 2882 (2008).
25. F. Samyn, S. Bourbigot, C. Jama, and S. Bellayer, *Polym. Degrad. Stabil.*, **93**, 2019 (2008).
26. F. Samyn, S. Bourbigot, C. Jama, S. Bellayer, S. Nazare, R. Hull, A. Fina, A. Castrovinci, and G. Camino, *Eur. Polym. J.*, **44**, 1631 (2008).
27. T. Kashiwagi, R. H. Harris, X. Zhang, R. M. Briber, B. H. Cipriano, S. R. Raghavan, W. H. Awad, and J. R. Shields, *Polymer*, **45**, 881 (2004).
28. X. Zhang and L. S. Loo, *Polymer*, **50**, 2643 (2009).
29. A. Leszczyńska, J. Njuguna, K. Pielichowski, and J. R. Banerjee, *Thermochim. Acta*, **453**, 75 (2007).
30. L. Haurie, A. I. Fernández, J. I. Velasco, J. M. Chimenos, J. M. L. Cuesta, and F. Espiell, *Polym. Degrad. Stabil.*, **92**, 1082 (2007).
31. F. Laoutid, P. Gaudon, J. M. Taulemesse, J. L. Cuesta, J. I. Velasco, and A. Piechaczyk, *Polym. Degrad. Stabil.*, **91**, 3074 (2006).
32. Y. Y. Yen, H. T. Wang, and W. J. Guo, *Polym. Degrad. Stabil.*, **97**, 863 (2012).
33. B. B. Marosfoi, S. Garas, B. Bodzay, F. Zubonyai, and G. Marosi, *Polym. Adv. Tech.*, **19**, 693 (2008).
34. J. Zhang, M. A. Delichatsios, and S. Bourbigot, *Combust. Flame.*, **156**, 2056 (2009).
35. S. Bourbigot, F. Samyn, T. Turf, and S. Duquesne, *Polym. Degrad. Stabil.*, **95**, 320 (2010).
36. J. W. Gilman, *Appl. Clay. Sci.*, **15**, 31 (1999).
37. A. B. Morgan, L. L. Chu, and J. D. Harris, *Fire Mater.*, **29**, 213 (2005).
38. B. Schartel and T. R. Hull, *Fire Mater.*, **31**, 327 (2007).
39. M. Lewin, *Polym. Degrad. Stabil.*, **88**, 13 (2005).
40. R. A. Vaia, G. Price, P. N. Ruth, H. T. Nguyen, and J. Lichtenhan, *Appl. Clay Sci.*, **15**, 67 (1999).
41. H. Lu, Y. Hu, J. Xiao, Z. Wang, Z. Chen, and W. Fan, *J. Mater. Sci.*, **41**, 363 (2006).
42. X. Hao, G. Gai, J. Liu, Y. Yang, Y. Zhang, and C. Nan, *Mater. Chem. Phys.*, **96**, 34 (2006).
43. Y. Hu, S. Wang, Z. Ling, Y. Zhuang, Z. Chen, and W. Fan, *Macromol. Mater. Eng.*, **288**, 272 (2003).
44. S. Pavlidou and C. D. Papaspyrides, *Prog. Polym. Sci.*, **33**, 1119 (2008).
45. W. S. Chow, A. A. Bakar, Z. M. Ishak, J. Karger-Kocsis, and U. S. Ishiaku, *Eur. Polym. J.*, **41**, 687 (2005).
46. C. M. Kim, D. H. Lee, B. Hoffmann, J. Kressler, and G. Stoppelmann, *Polymer*, **42**, 1095 (2001).
47. L. Lepluart, J. Duchet, and H. Sautereau, *Polymer*, **46**, 12267 (2005).
48. T. D. Fornes and D. R. Paul, *Polymer*, **44**, 3945 (2003).
49. J. Ma, S. Zhang, Z. Qi, G. Li, and Y. Hu, *J. Appl. Polym. Sci.*, **83**, 1978 (2002).
50. J. W. Lim, A. Hassan, A. R. Rahmat, and M. U. Wahit, *Polym. Int.*, **55**, 204 (2006).
51. H. Balakrishnan, M. Ibrahim, M. U. Wahit, and A. Hassan, *Polym. Compos.*, **32**, 1927 (2011).
52. D. Tomova, J. Kressler, and H. J. Radusch, *Polymer*, **41**, 7773 (2000).